

Human-Centered Stability Augmentation Control for a Hip Exoskeleton Under Leaning and Slip Perturbations

Abstract—The vast majority of existing control paradigms for lower-limb exoskeletons are developed and validated under steady-state locomotor tasks. Their performance under unstable conditions or external perturbations remains largely unexplored. Moreover, existing controllers for gait stability augmentation are often task-specific, reference kinematics dependent, and largely reactive rather than proactive in responding to instability, which can limit their generalization and restrict users’ voluntary motion. In this paper, we propose a control paradigm for lower-limb exoskeletons to provide proactive stability assistance while preserving individual preferences. The paradigm first defines a center of mass-based stability indicator, and then enforces its dynamics to remain within a user-specific safe range through control barrier functions. The safety set triggers corrective assistance as the user’s state approaches the boundary to enable proactive support. To account for voluntary human motion, we propose a nonlinear disturbance observer to estimate human joint torques and incorporate them into the control design. Experiments with two non-disabled subjects wearing a bilateral hip exoskeleton demonstrate the effectiveness of the proposed approach in leaning and randomized slip perturbations. Experimental results show that ensemble-averaged muscle efforts decreased by 41% (leaning) and 24% (slipping), along with lower peak-to-peak whole-body angular momentum and faster recovery. These preliminary results demonstrate the potential of the proposed control paradigm to augment gait stability across diverse unstable scenarios.

I. INTRODUCTION

Falls and related injuries impose a major public health burden across all ages. Globally, falls caused over 600,000 deaths in a year [1]. Among the major causes of falls, slip events account for approximately 40% of outdoor falls in elderly individuals and can lead to severe injuries such as hip fracture [2]. Traditional assistive devices such as canes/walkers and ankle-foot orthoses primarily provide passive support to improve balance [3]. However, their effectiveness and adaptability are often limited in practice. For example, canes and walkers require constant hand grasping, which can restrict upper-limb motion and reduce mobility. Similarly, while passive ankle-foot orthoses can improve certain gait stability metrics in clinical populations, they are typically designed to restrict plantarflexion and dorsiflexion, thereby limiting ankle motion during stance [4]. In contrast, emerging powered lower-limb exoskeletons have shown strong potential for both rehabilitation [5] and daily assistance [6]. Beyond assisting steady-state locomotion, their ability to provide active joint-level assistance and highly customized support [6] also makes them promising for gait stability.

A variety of exoskeleton-based strategies have been proposed to enhance safety and stability, yet important limitations remain. For example, a “help-when-needed” time-dependent

controller was developed to assist balance recovery [7], but its pre-defined torque profiles do not account for users’ voluntary responses during a fall. Capture point theory has also been used to correct unsafe leaning and prevent falls [8], and Zhu et al. further designed a controller based on slip recoverability regions to assist recovery after unexpected foot slips [9]. Although effective in their targeted scenarios, these approaches generally rely on pre-defined reference kinematics or equilibrium joint configurations, which can limit generalization across locomotion scenarios and overly constrain voluntary motion. A momentum-based controller was later formulated as a constrained quadratic program to generate torques that minimize momentum changes without enforcing pre-defined reference kinematics [10]. However, its standing-specific constraints limit its applicability to broader locomotion tasks. In parallel, center of mass (CoM)-based methods are widely used for gait stability assessment and control. For instance, the extrapolated center of mass (XCoM) has been used to provide balance assistance by enforcing the CoM within the support polygon [11]. However, XCoM is derived from a linear inverted pendulum model with a fixed eigenfrequency, and its assumption of constant CoM height may break down in more dynamic locomotion tasks or under large perturbations.

Control barrier functions (CBFs) have gained attention as an efficient framework for safety-critical control given their low real-time computational cost [12]. They have been applied to applications ranging from dynamic balancing on a Segway-type robot [13] to real-time stable walking for bipedal robots [14]. More recently, CBFs have also been applied to improve gait safety by restricting the user’s gait-planning parameters within a pre-defined range [15]. However, since the safety range was specified using reference kinematics, the controller may still impose undue constraints on the user’s voluntary motion. Furthermore, since the CBF is not constructed from a whole-body stability and its temporal derivative, it cannot generate proactive corrective torques when the user state remains within the admissible set but is evolving rapidly toward the boundary of instability. Overall, a key open challenge is to develop a gait stability augmentation strategy that can assist diverse locomotion and perturbation scenarios without prescribing reference kinematics, while explicitly accounting for the user’s voluntary input.

In this paper, we propose a stability augmentation controller (SAC) that aims to improve gait stability without prescribing reference kinematics or overly interfering with a user’s voluntary motion, thereby offering the potential to generalize across diverse locomotor tasks and perturbations. To achieve this,

we first construct a CoM-based stability indicator by defining stable locomotion as maintaining the CoM state (position and velocity) within a stability-safe range relative to stance and swing feet. We then formulate stability augmentation as a safety-critical control problem and use CBFs to keep this indicator within its safe range during both steady-state locomotion and perturbations. Because the CoM is a weighted sum of all body segments, regulating it does not impose joint-level kinematic trajectories and therefore allows users to maintain stability using self-selected strategies. In addition, the CBF acts as a torque filter that minimally modifies the nominal control input to satisfy stability constraints, thereby reducing interference during steady-state motion while providing rapid corrective assistance when instability is detected. We further introduce relaxation terms in the stability indicator to preserve natural user responses under mild instability. By incorporating both position and velocity into the CBF formulation, the proposed SAC can also provide assistance before unstable postures fully develop when stability is deteriorating rapidly to enable more proactive assistance, which is beneficial in assisting users during balance recovery [16]. To explicitly consider human input and preserve voluntary motion, we also propose a nonlinear disturbance observer (NDO) for online estimation of human joint torques and incorporate them into control design.

To evaluate SAC's performance, we conducted experiments with two non-disabled subjects wearing a powered hip exoskeleton during quasi-static leaning tasks and walking tasks with randomly timed slip perturbations. Slip perturbations were selected because slips are among the most common causes of falls [2]. Moreover, treadmill-induced slips allow precise and repeatable control of perturbation timing and intensity, while still allowing voluntary human responses. The results showed average reductions in muscle effort of 41% during leaning and 24% during slipping, together with an 11% decrease in peak-to-peak whole-body angular momentum (WBAM) and shorter recovery time during slip perturbations. These results highlight the potential of SAC to provide partial assistance in reducing muscular demand and improving stability recovery under perturbations without prescribing kinematic trajectories.

The rest of the paper is organized as follows: Sec. II presents the dynamics of the human-exoskeleton system and briefly reviews the concept of CBFs. We then derive the controller using a CoM-based CBF and human joint input estimation using the NDO in Sec. III. The bilateral hip exoskeleton used for experimental validations is presented in Sec. IV, followed by the experimental model and protocol in Sec. V. We demonstrate experimental results in Sec. VI and draw conclusions in Sec. VII.

II. PRELIMINARIES

A. Dynamics of the Human-Exoskeleton System

We model a human walking with an exoskeleton as one biped, with its dynamics expressed as [17]

$$M\ddot{q} + C\dot{q} + N + A^T\lambda = \tau + J^T F_{\text{perturb}}, \quad (1)$$

where $q \in \mathbb{R}^n$ is the vector of generalized coordinates, n is the number of degrees of freedom (DoFs), $M \in \mathbb{R}^{n \times n}$ denotes the inertia matrix, $C \in \mathbb{R}^{n \times n}$ is the Coriolis/centrifugal matrix, and $N \in \mathbb{R}^n$ represents the gravitational forces vector. The constraint matrix A , which is the gradient of holonomic contact constraints, maps the ground reaction forces $\lambda = \hat{\lambda} + \dot{\lambda}\tau$ into the overall dynamics, where $\hat{\lambda} = W(\dot{A}\dot{q} - AM^{-1}N)$, $W = (AM^{-1}A^T)^{-1}$, and $\dot{\lambda} = WAM^{-1}$ [17]. In (1), the inertial parameters represent the combined human-exoskeleton system, with the human inertial parameters estimated using the method in [18]. The overall torque τ combines human joint torque vector τ_{hum} and exoskeleton torque vector $\tau_{\text{exo}} = Bu$, where $B = (0_{p \times (n-p)}, I_{p \times p})^T \in \mathbb{R}^{n \times p}$ maps the exoskeleton torque $u \in \mathbb{R}^p$ into the dynamics with p as the number of exoskeleton actuators. We explicitly account for all potential external perturbation forces by introducing a wrench $F_{\text{perturb}} \in \mathbb{R}^6$ and mapping it into the dynamics via a Jacobian matrix $J \in \mathbb{R}^{6 \times n}$.

B. Review of Control Barrier Functions

The general form of a nonlinear system can be written as

$$\dot{x} = f(x) + g(x)u, \quad (2)$$

where $x \in \mathcal{D} \subset \mathbb{R}^j$ represents the state vector, $f(\cdot)$ and $g(\cdot)$ are locally Lipschitz functions. Choosing the system state $x = [q^T, \dot{q}^T]^T \in \mathbb{R}^{2n}$, the biped dynamics (1) can be formulated in the form of (2), *i.e.*,

$$\dot{x} = f(x) + g(x)u = \begin{bmatrix} \dot{q} \\ M^{-1}Q \end{bmatrix} + \begin{bmatrix} 0 \\ M^{-1}B \end{bmatrix} u, \quad (3)$$

where $Q = -C\dot{q} - N - A^T\lambda + \tau_{\text{hum}} + J^T F_{\text{perturb}}$. A safe set $\mathcal{C} = \{x \in \mathcal{D} \subset \mathbb{R}^j : h(x) \geq 0\}$ is a closed set that consists of all admissible safe states defined by a continuously differentiable barrier function $h(x) : \mathcal{D} \rightarrow \mathbb{R}$. With this definition, the system can be considered safe if the set \mathcal{C} is asymptotically stable and forward-invariant in \mathcal{D} . Assume h (with x omitted hereafter) has relative degree one, it is a CBF if there exists an extended class \mathcal{K}_∞ function α such that for (2) and for all $x \in \mathcal{D}$,

$$\sup_{u \in \mathcal{U}} [L_f h + L_g h u] \geq -\alpha(h), \quad (4)$$

where $L_f h$ and $L_g h$ denote Lie derivatives [19]. Any Lipschitz continuous controller u chosen from

$$K_{\text{cbf}}(x) = \{u \in \mathcal{U} : L_f h + L_g h u + \alpha(h) \geq 0\} \quad (5)$$

ensures that the set \mathcal{C} is forward-invariant and asymptotically stable in \mathcal{D} , thereby guaranteeing safety. When a CBF is formulated based on an individual's gait stability, the control input selected from (5) can be used to enhance gait stability.

III. CONTROL DESIGN

In this section, we design a CBF-based control paradigm to augment the balance of human walking under unstable postures or external perturbations. In particular, unlike conventional kinematics-based methods [15], the proposed paradigm regulates whole-body dynamics while being grounded in

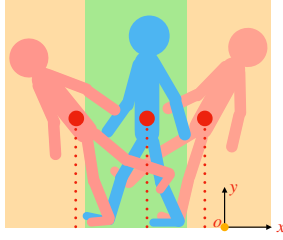


Fig. 1: Illustration of the safety indicator in (6). The red dots denote the CoM, and the green/yellow regions represent the stability-safe/unstable ranges of the indicator.

joint-level local kinematic information. This structure enables instability detection and corresponding assistance, while accommodating user preference by explicitly incorporating human torques into the control design.

A. CoM-Based Control Barrier Function

To design a CBF for stability augmentation, we first need an indicator that can continuously quantify gait stability. A common choice is the XCoM, which is widely used in gait analysis and stability control [11]. For instance, the margin of stability (MoS) [20] measures stability as the signed distance between the XCoM and the boundary of the base of support (BoS), with positive values indicating stable walking. However, because XCoM is derived from a simplified inverted pendulum model with an approximately constant CoM height assumption, its validity can degrade under large perturbations. Motivated by the BoS-margin interpretation of MoS, we instead define a CoM-based CBF that incorporates tolerance for natural gait variations and user-specific stabilization strategies. We first define a stability indicator

$$s = [\text{CoM}_x - (x_- - \delta_1)][(x_+ + \delta_2) - \text{CoM}_x], \quad (6)$$

where CoM_x denotes the horizontal position of CoM, x_- and x_+ are the horizontal positions of posterior and anterior foot boundaries, respectively:

$$x_- = \min(p_{st,x}, p_{sw,x}), \quad x_+ = \max(p_{st,x}, p_{sw,x}), \quad (7)$$

where $p_{st,x}$ and $p_{sw,x}$ indicate the horizontal positions of the outer boundaries associated with the stance and swing feet. In (6), $\delta_1, \delta_2 \geq 0$ are the relaxation terms that expand the stability margin to tolerate natural gait variation and user-specific stabilization strategies. The proposed indicator defines gait stability as the swing leg's ability to capture the destabilized body (Fig. 1), as the swing leg advances to arrest the body's forward fall at the onset of next step [21]. Finally, we define a relative-degree one CBF that considers both the value of s and its derivative, *i.e.*,

$$h = \gamma_1 s + \gamma_2 \dot{s} + c, \quad (8)$$

where $\gamma_1, \gamma_2 > 0$ control the contribution of s and \dot{s} to h [22], $c \geq 0$ is a relaxation term that allows the user to approach or slightly deviate from the safe set and to accommodate user-specific stabilization strategies. We can see from (6) and (8) that although h has a similar form to XCoM [11], its

design provides the flexibility for parameter tuning to account for user preferences.

With the CBF defined in (8), we now incorporate it into an optimization procedure to determine the SAC, *i.e.*,

$$\begin{aligned} \min_u \quad & u^T W u \\ \text{s.t.} \quad & L_f h + L_g h u \geq -\alpha(h), \end{aligned} \quad (9)$$

where W is a diagonal, positive definite weight matrix, and $\alpha(\cdot)$ is an extended class \mathcal{K}_∞ function. The control strategy not only considers kinematic relations between CoM and feet locations, it also incorporates human input τ_{hum} , whose estimation will be introduced next.

B. Human Joint Torque Estimation via NDO

Solving u from (9) requires the knowledge of human joint torque τ_{hum} to calculate $L_f h$, which can be hard to measure directly in practice. To address this, we propose a novel NDO [23] to estimate a modified term of human input and the external perturbations $M^{-1}[(I - A^T \dot{\lambda})\tau_{\text{hum}} + J^T F_{\text{perturb}}]$ based on joint information through Euler-Lagrange dynamics. We estimate the modified term rather than τ_{hum} directly because the modified term appears in (9) and directly estimating τ_{hum} can be sensitive to small eigenvalues of M . Left multiplying M^{-1} on both sides of (1) yields

$$\ddot{q} + M^{-1}(C\dot{q} + N + A^T \dot{\lambda}) = M^{-1}B_\lambda u + z. \quad (10)$$

Here, $z = M^{-1}[(I - A^T \dot{\lambda})\tau_{\text{hum}} + J^T F_{\text{perturb}}]$ represents the “disturbance” term to be estimated, and $B_\lambda = (I - A^T \dot{\lambda})B$. Note that when a perturbation is present, the “disturbance” term would consist of both human input and the external perturbation forces. Rewrite (10) as

$$z = \ddot{q} + M^{-1}(C\dot{q} + N + A^T \dot{\lambda} - B_\lambda u). \quad (11)$$

Defining \hat{z} to be the estimate of z , we have:

$$\begin{aligned} \dot{\hat{z}} &= L(z - \hat{z}) \\ &= -L\hat{z} + L[\ddot{q} + M^{-1}(C\dot{q} + N + A^T \dot{\lambda} - B_\lambda u)], \end{aligned} \quad (12)$$

where $L \in \mathbb{R}^{n \times n}$ is a diagonal, positive definite matrix to be designed. During implementation, \hat{z} can be numerically updated as $\hat{z}_{k+1} = \hat{z}_k + \Delta t l(\hat{z}_k, q_k, \dot{q}_k, \ddot{q}_k, u_k)$, where Δt is the sampling period and $l(\hat{z}_k, q_k, \dot{q}_k, \ddot{q}_k, u_k)$ represents the right-hand side of (12) evaluated at the current states and control input. Assuming the change rate of z is bounded, we can guarantee that the estimation error $e = z - \hat{z}$ is uniformly ultimately bounded [24].

IV. BILATERAL HIP EXOSKELETON SYSTEM

We conducted human subject experiments on a bilateral, powered hip exoskeleton (Enhanced Power Technology Co., Ltd., Shenzhen, China, Fig. 2, left) equipped with externally mounted inertial measurement units (IMUs) and a Raspberry Pi board (Fig. 2, right). We selected this device for two main reasons. The hip joint plays a key role in recovering from slips [25], and thus providing assistance at the hip joint could bring benefits in augmenting gait stability. On the other hand, the compact and lightweight design of the

exoskeleton aligns with our control objective, *i.e.*, providing partial assistance on top of human’s natural reactions. In this section, we present the exoskeleton hardware, the external sensors used for kinematics measurements, and the overall control architecture.

A. Hip Exoskeleton

The exoskeleton has two brushless DC motors, each of which can deliver 7.5 Nm rated torque and 22.5 Nm peak torque with a 25:1 gear ratio. The system achieves a low backdrive torque of 0.096 Nm to allow for voluntary human movements. The actuator system enables current regulation at 400 Hz through a GD32F303RE microprocessor (ARM Cortex-M4, 120 MHz, 512 kB ROM, 64 kB RAM) along with two joint encoders and current sensors. All electrical components are powered by an onboard 3200 mAh lithium battery.

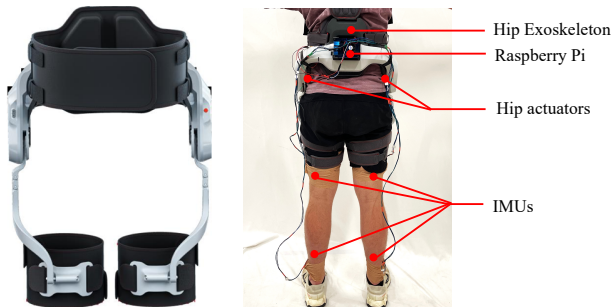


Fig. 2: Left: The powered hip exoskeleton. Right: A subject wearing the exoskeleton with externally mounted IMUs and a Raspberry Pi.

B. Human Kinematics Measurements

We measured ankle, knee and hip orientations of subjects at 200 Hz using four IMUs (NGIMU, x-io Technologies Ltd., Bristol, UK) placed at their thighs and shanks. The IMUs used a built-in Attitude and Heading Reference System fusion algorithm [26] for signal smoothing. The joint angles were then transmitted to a Raspberry Pi 4B (8GB LPDDR4-3200 SDRAM, Cortex-A72 64-bit SoC, 1.8 GHz) over UART and then differentiated along with a 71-sample moving average filter [27] for NDO and SAC calculation.

C. Control Architecture

The overall control structure consists of two loops: a high-level loop that handles communication and real-time computation, and a low-level loop that realizes torque control (Fig. 3). We used a Raspberry Pi to communicate with the IMUs and the exoskeleton, estimate real-time human input using the NDO, and compute u via (9) by an open-source, lightweight quadratic programming solver, Operator Splitting Quadratic Program (OSQP) [28]. The resulting torque command is transmitted to the exoskeleton via UART, where the embedded motor driver (ER-Driver) regulates actuator current to realize the desired torque through a torque constant of 0.083 Nm/A. Although the control algorithm can run at 300 Hz on the Raspberry Pi, the update rate was limited to 150 Hz during experiments to match the exoskeleton’s communication frequency.

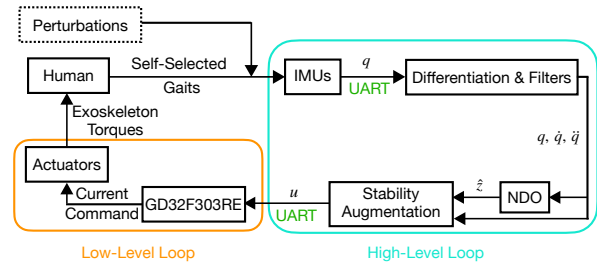


Fig. 3: Overall structure of the exoskeleton control system.

V. EXPERIMENTAL STUDY

A. Experimental Model

Because ankle joints play a relatively minor role in stability recovery [25] and a hip exoskeleton does not directly assist ankle joints, we adopted a 4-DoF, no-feet model for experiments (Fig. 4) to ensure a manageable computational burden on the Raspberry Pi. The configuration vector is given as $q = (\phi, \theta_k, \theta_h, \theta_{sk})^T \in \mathbb{R}^4$, where ϕ is the global orientation of stance shank, and θ_i , $i \in \{k, h, sk\}$ denote the relative angles of stance knee, hip, and swing knee, respectively. Since the model assumes no-slip stance foot contact, the constraint force λ can be eliminated in (1), yielding $B_\lambda = B$ in (10) [17]. During slip perturbations, this assumption is transiently violated. However, because such violation is brief, the simplified model remains a reasonable local approximation for control synthesis. The resulting mismatch is treated as a transient disturbance and estimated through the NDO.

The experimental model is formulated based on an inertial reference frame (IRF) fixed at the user’s stance foot. To accommodate IRF shifts during stance leg switches, we maintained two identical 4-DoF models, each anchored to one foot. During experiments, the model corresponding to the current stance leg is used to compute u , which is then applied to the ipsilateral hip actuator. We split u equally between the two actuators, which is supported by the approximately symmetric hip torque profiles for steady-state walking [18], and an individual’s recovery strategies are approximately invariant to perturbation side [29]. Our experimental results will demonstrate that during perturbations, this equal torque distribution helped stabilize the stance leg while advancing the swing leg, thereby reducing their muscle activities in Sec. VI. During experiments, we saturated the actuator torques at ± 15 Nm to avoid excessive torques, meanwhile able to provide adequate recovery assistance.

B. Experimental Protocol

Two non-disabled subjects (s1: 20 yr, 76.0 kg, 1.83 m; s2: 34 yr, 102.5 kg, 1.80 m) were recruited for experiments, where preliminary validation with the same sample size can be found in [30]. The experimental protocol was approved by the authors’ Institutional Review Board, and written informed consent was obtained prior to data collection.

At the start of the experiments, the subjects were asked to walk on the treadmill at 0.8, 1.0, and 1.2 m/s for 30 seconds under passive mode (PAS, exoskeleton worn but actuators

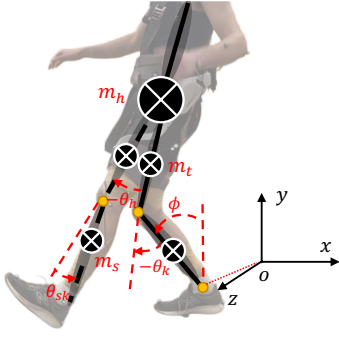


Fig. 4: A representative backward slipping posture of a subject along with the 4-DoF model used for experimental implementation. The trunk and hip are lumped into a single point mass.

off). These data were used to tune subject-specific SAC parameters (δ_1 , δ_2 , γ_1 , γ_2 , and c) such that SAC remained effectively inactive during steady-state walking, and remained unchanged for the remainder of the experiments. After passive trials, each subject completed two sessions of experiments: 1) forward leaning (FL)/backward leaning (BL), and 2) forward slipping (FS)/backward slipping (BS) sessions, with details summarized in Fig. 5. For leaning trials, the subject stood still while the treadmill started to slowly move to induce a gradual forward (FL) or backward (BL) lean. The subject was instructed to keep their feet stationary until a reactive step was necessary to recover balance. To ensure consistency across subjects and trials, subjects were instructed to respond with their right legs. For slipping trials, we simulated slip-like perturbations by triggering a sudden anteroposterior treadmill belt acceleration or deceleration at heel contacts after a random number of steady-state steps [31]. For the slipping session, the order of perturbation directions and onset timing and control conditions was randomized to prevent anticipation.

For all experiments, we chose $\alpha(h) = 0.1h^3$ from pilot trials, aiming to generate rapid control input response for unstable postures, W as an identity matrix, and $L = 100 \cdot I_{4 \times 4}$ in the NDO to achieve rapid convergence of the estimated torque while maintaining consistent magnitude with Winter's hip torque profile [18] from simulation study [24]. During slip trials, we additionally implemented a momentum regulation controller (MRC) [24] that provides benefits in muscular efforts during steady-state locomotion for comparison. This controller continuously regulates an individual's WBAM, a widely used stability metric in locomotion, to provide a complementary baseline to SAC. Throughout the experiments, the subject wore an overhead harness to ensure safety, and its height was adjusted to avoid interference during walking.

We collected 10 (leaning) and 12 (slipping) SAC trials in total. For quantitative analysis, we used fixed subsets (5 leaning, 6 slipping) with consistent inclusion criteria (complete EMG/marker data, no trajectory failures, and reliable actuator execution). These criteria were applied uniformly across subjects and conditions and did not alter the reported trends. For leaning trials, the analysis window spanned from reactive step onset to foot strike of the stepping foot when stability was regained. For slipping trials, the perturbation

interval was defined from the heel strike immediately before treadmill acceleration/deceleration to the second heel strike of the same foot afterward, by which point WBAM indicated restoration of stable gait.

C. Muscle Activities and Kinematic Measurements

We measured and recorded the Rectus Femoris (RF), Biceps Femoris (BF), Gluteus Medius (GMed), and Gluteus Maximus (GMax) of each subject via electromyographic (EMG) sensors (Delsys Inc., MA). These muscles were selected because RF primarily acts as a hip flexor, BF as a primary hip extensor, GMed as the primary hip abductor with a secondary role in hip extension/stabilization, and GMax as a major hip extensor [21], which are related to strategies for maintaining and recovering gait stability during slip perturbations [32], [33]. The EMG data was first filtered by a 4th-order band-pass filter with a 20-500 Hz passband and rectified, and then filtered by a low-pass filter with 6 Hz cutoff frequency. The EMG data was then normalized with respect to the maximum peak EMG values throughout walking trials, thereby converting the signals to a percentage of the peak filtered EMG values.

We also recorded the subjects' body movements via a motion capture system (Vicon, Oxford, UK) with a modified 30-marker Plug-in-Gait Full Body model [34]. Marker trajectories were sampled at 100 Hz and imported into OpenSim using a scaled musculoskeletal model (22 rigid bodies, 37 DoFs [35]). The subjects' WBAM was then computed from the resulting kinematic data.

VI. RESULTS & DISCUSSION

In this section, we present the estimated human hip torques, exoskeleton torques and the associated safety indicator values, muscle activations, and WBAM results in Figs. 6 to 10. In all gait-cycle plots, 0% denotes stance leg heel strike, and 100% represents the subsequent strike of the same leg. For leaning trials, 0% and 100% denote the start and end of the perturbation intervals, respectively. Positive/negative torques correspond to hip extension/flexion, respectively.

A. NDO, Exoskeleton Torques, and Stability Indicator

The NDO-estimated hip torque is shown in Fig. 6. It closely matches the waveform and magnitude reported in Winter's normative gait dataset [18], showcasing the estimation accuracy of the proposed NDO, even with the 4-DoF model.

Sample exoskeleton torques along with the corresponding s values are shown in Fig. 7. The torques remained near zero during stable postures and increased rapidly following the onset of instability caused by excessive leaning angles or the onset of slip perturbations, which are successfully detected by the proposed stability indicator (with s approaching zero or becoming negative) in all scenarios. Notably, the proposed controller generated distinct torque profiles and directions across perturbation conditions without pre-specifying a torque waveform, suggesting good adaptability to different perturbation scenarios.

During leaning trials, the delay between exoskeleton torque onset and the unstable postures ($s < 0$) arises from the

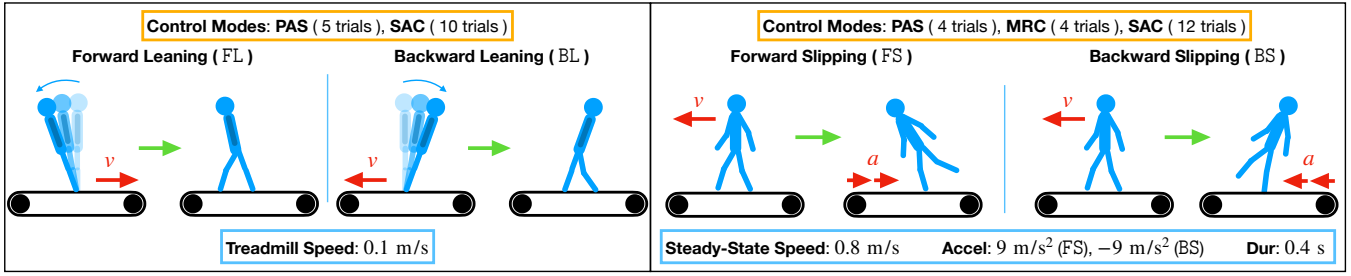


Fig. 5: Summary of experimental setup and conditions.

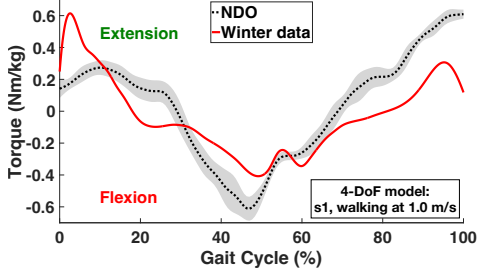


Fig. 6: Estimated hip torque (mean \pm 1-SD) compared with Winter's dataset.

relaxation term in (8), which keeps h positive under mildly unstable conditions. This allows small deviations from the nominal safe region, allowing voluntary responses and user-specific stabilization strategies. In contrast, during slipping trials, the exoskeleton torque was activated before s became negative, as highlighted by the green box in Fig. 7. This earlier onset is due to two features of the CBF design. First, \dot{s} in (8) captures the evolution of stability, so rapid perturbations can drive the system toward an unsafe condition even before s becomes negative. Second, the selected $\alpha(h)$ in (9) allows \dot{h} to be slightly negative when h is positive but near zero. As a result, when human effort alone is insufficient during large slip perturbations, the controller provides torques preemptively to prevent potential gait instability. Together, these mechanisms enable SAC to assist before an unstable posture fully develops, which is often required as shown in previous studies [16].

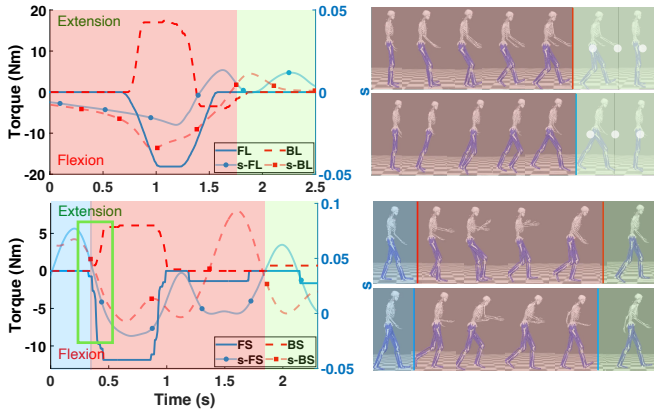


Fig. 7: Sample swing leg exoskeleton torques of s_1 along with stability indicator value (s) and related postures during leaning (top) and slipping trials (bottom). Blue/red/green shaded areas indicate the pre-, during-, and post-perturbation intervals, respectively.

B. EMG & Muscular Efforts

The ensemble-averaged normalized EMG patterns for leaning trials are shown in Fig. 8. Overall, all recorded muscles show consistently lower activities with SAC compared to PAS, indicating that the SAC torques can effectively offload the subjects' muscle activities during the recovery. Specifically, during FL trials, the subject flexed the right hip joint (swing side) and thus moved the right leg forward to complete a step and catch the forward-falling body. Accordingly, the right RF, a hip flexor, became highly active, and the right-hip flexion exoskeleton torque (Fig. 7) reduced the biological hip flexion demand to offload the right RF activation [32]. In contrast, the corresponding left-hip (stance side) extension exoskeleton torques helped prevent the pelvis and trunk from pitching forward, thus reduced the required stance hip extensor effort, leading to a large decrease in the left GMax. Moreover, according to the subjects' feedback, the left-hip extension exoskeleton torque assisted them in stabilizing their stance legs, and thus could reduce stabilization demand on GMed [33]. Similarly, during BL trials, the right-hip extension exoskeleton torque reduced the need for right hip extensor during the recovery step, resulting in reduced activation of right RF, BF, and GMax compared with PAS.

For slipping trials, subjects exhibited varying stability recovery strategies, leading to trial- and subject-specific variations in EMG waveforms. To better demonstrate the efficacy of assistance on muscle activities, we reported the average normalized integrated EMG (iEMG) across subjects and trials in Fig. 9. Overall, compared with PAS and MRC modes, SAC yielded lower iEMG values in almost all recorded muscles during both FS and BS trials, suggesting that SAC can effectively offload the subjects' muscle activities during slip perturbations. In particular, SAC reduced iEMG in the hip extensors and flexors (RF, GMax, and BF), indicating offloading of the hip demands needed for transient rapid stability recovery. The reduced GMed activity further highlights decreased hip stabilization effort [33]. In contrast, MRC generally increased iEMG across muscles, suggesting that WBAM regulation during slip did not effectively mitigate fall risks, and control strategies designed for steady-state walking did not naturally translate to effective recovery strategies under perturbations.

For each subject, muscle effort was defined as the averaged normalized iEMG of all recorded muscles over the perturbation interval, computed across all trials [36]. We then computed the ensemble-average muscle effort by averaging

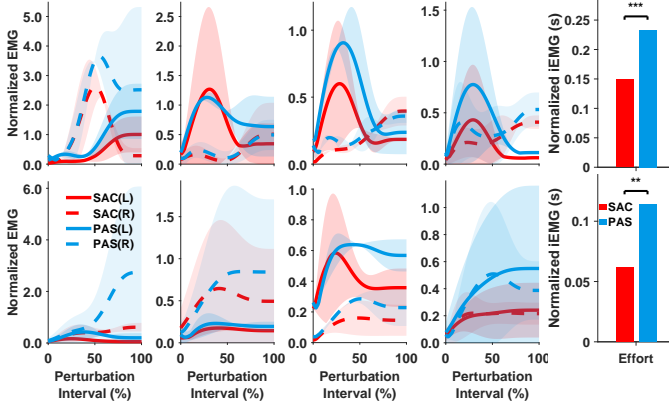


Fig. 8: Ensemble-averaged normalized EMG (mean \pm 1·SD) for subjects s1 and s2 in FL (top) and BL (bottom). From left to right are RF, BF, GMed, GMax, and muscle efforts. Statistical significance was tested using mixed-effects analysis of variance (ANOVA, ** $P \leq 0.01$, *** $P \leq 0.001$).

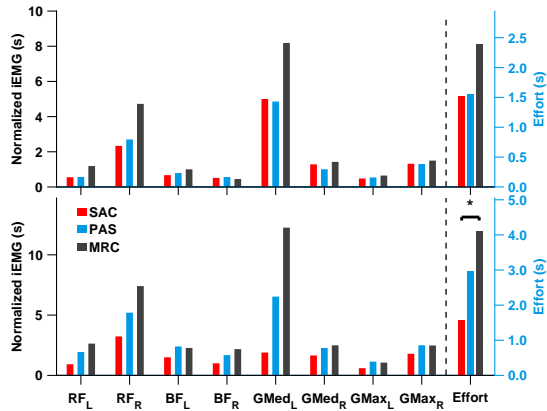


Fig. 9: Ensemble-averaged muscle activities and efforts (top: FS, bottom: BS), * indicates $P \leq 0.05$.

the subject-level muscle effort values across both subjects:

$$\text{Effort} = \frac{1}{2} \cdot \frac{1}{8} \cdot \frac{1}{n_{\text{mode}}} \sum_k \sum_t \sum_i \frac{i\text{EMG}_{i,t,k}}{\text{EMG}_{\text{max},i,k}}, \quad (13)$$

where n_{mode} denotes the number of trials within a control mode, $i\text{EMG}_{i,t,k}$ is the $i\text{EMG}$ of muscle i for subject k in trial t , with $i \in \{\text{RF}, \text{BF}, \text{GMed}, \text{GMax}\}$ for both legs, and $\text{EMG}_{\text{max},i,k}$ denotes the maximum EMG value of subject k 's muscle i during steady-state walking. The fractions $\frac{1}{2}$ and $\frac{1}{8}$ in (13) denote averaging over the two subjects and the eight recorded muscles, respectively. The results are shown in the right-hand side of Figs. 8 and 9. On average, compared to PAS, SAC reduced subjects' muscular efforts by 35.99%, 45.96%, 1.31%, and 46.80% in FL, BL, FS, and BS trials, respectively. Overall, these results indicate that SAC can consistently offload muscle activities while maintaining stability recovery during slips.

C. Whole-Body Angular Momentum

WBAM has been frequently used to evaluate gait stability [37]. Unstable or perturbed gaits tend to result in larger WBAM deviations compared to steady-state walking [38]. We reported the individual and ensemble-averaged sagittal WBAM of both subjects in Fig. 10. The slip perturbations

resulted in noticeable WBAM deviations relative to steady-state walking, followed by a recovery toward steady oscillations. Compared with PAS and MRC, SAC consistently reduced the maximum WBAM deviations in both FS and BS trials. Quantitatively, compared with PAS, SAC reduced the peak-to-peak WBAM by 4.26% and 17.50% on average during FS and BS trials, respectively. The larger reduction observed in BS trials could reflect SAC's effectiveness under more challenging conditions, i.e., backward slips (based on subjects' feedback). In contrast, PAS and MRC tended to result in larger WBAM peaks or prolonged deviations during the post-perturbation phase, suggesting less effective stability recovery performance compared with SAC.

To further evaluate the proposed control strategy in restoring gait stability, we computed the average WBAM-based recovery time (Fig. 10), following the general "return-to-baseline and remain" concept [39]. In general, shorter recovery time represents faster recovery to steady-state walking after perturbation and thus is preferred. In Fig. 10, SAC reduced the mean recovery time in all conditions. The MRC, however, tended to increase the mean recovery time in most conditions. Together with peak-to-peak WBAM and muscle activity, benefits of MRC seem more condition-dependent. Overall, compared with PAS and MRC, the proposed SAC effectively reduces the slip-induced peak-to-peak WBAM and mean gait recovery time.

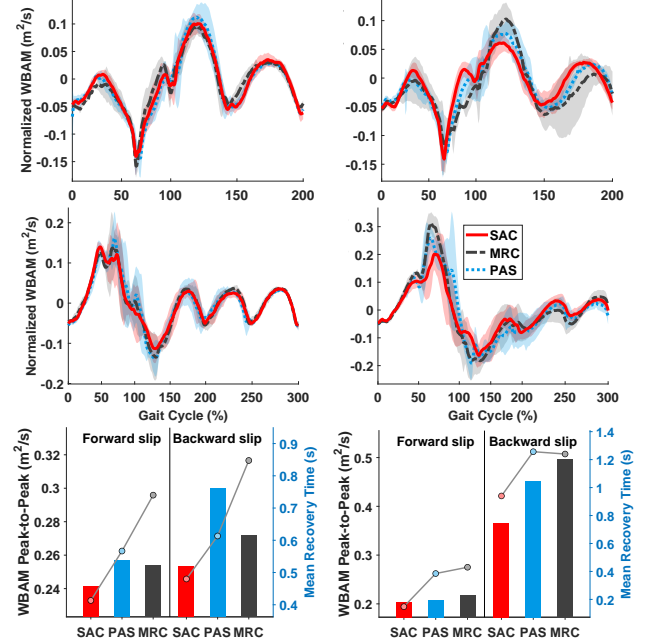


Fig. 10: Mean \pm 1·SD individual sagittal WBAM of s1 (left) and s2 (right) in FS (top), BS (middle), and bar plots of average peak-to-peak WBAM with recovery time (bottom).

VII. CONCLUSION

This paper presents a stability augmentation control paradigm to augment gait stability under unstable postures or external perturbations. The proposed approach first defines a CoM-based stability indicator, and enforces it to remain within a safe range defined over the stability indicator and its

temporal derivative using CBFs. The proposed approach does not prescribe reference kinematics, and assistance is proactive and triggered when gait stability is approaching or exceeding the defined safe set. To explicitly account for human voluntary inputs, we proposed an NDO to estimate human joint torques in real time. Experimental results with two non-disabled subjects performing quasi-static leaning tasks and steady-state walking under slip perturbations validate the effectiveness of the proposed method in reducing muscular efforts, lowering perturbation-induced peak-to-peak WBAM, and shortening the average recovery time. Future work will integrate SAC with existing controllers for steady-state walking to enable seamless assistance across both nominal and unstable gait conditions.

REFERENCES

- [1] S. L. James, L. R. Lucchesi, C. Bisignano, C. D. Castle, Z. V. Dingels, J. T. Fox, E. B. Hamilton, N. J. Henry, K. J. Krohn, Z. Liu *et al.*, "The global burden of falls: global, regional and national estimates of morbidity and mortality from the global burden of disease study 2017," *Inj. Prev.*, vol. 26, no. Suppl 2, pp. i3–i11, 2020.
- [2] Y. Wang, T. Bhatt, X. Liu, S. Wang, A. Lee, E. Wang, and Y.-C. C. Pai, "Can treadmill-slip perturbation training reduce immediate risk of over-ground-slip induced fall among community-dwelling older adults?" *J. Biomech.*, vol. 84, pp. 58–66, 2019.
- [3] D. Adiputra, N. Nazmi, I. Bahiuddin, U. Ubaidillah, F. Imaduddin, M. A. Abdul Rahman, S. A. Mazlan, and H. Zamzuri, "A review on the control of the mechanical properties of ankle foot orthosis for gait assistance," in *Actuators*, vol. 8, no. 1. MDPI, 2019, p. 10.
- [4] M. A. Brehm, J. Harlaar, and M. Schwartz, "Effect of ankle-foot orthoses on walking efficiency and gait in children with cerebral palsy," *J. Rehabil. Med.*, vol. 40, no. 7, pp. 529–534, 2008.
- [5] B. Johnson and M. Goldfarb, "A preliminary study on the feasibility of using a knee exoskeleton to reduce crouch gait in an adult with cerebral palsy," in *Int. Conf. Biomed. Robot. Biomechatronics*. IEEE, 2020, pp. 48–53.
- [6] R. Baud, A. R. Manzoori, A. Ijspeert, and M. Bouri, "Review of control strategies for lower-limb exoskeletons to assist gait," *J Neuroeng Rehabil*, vol. 18, no. 1, pp. 1–34, 2021.
- [7] V. Monaco, P. Tropea, F. Aprigliano, D. Martelli, A. Parri, M. Cortese, R. Molino-Lova, N. Vitiello, and S. Micera, "An ecologically-controlled exoskeleton can improve balance recovery after slippage," *Sci. Rep.*, vol. 7, no. 1, p. 46721, 2017.
- [8] M. Deng, Z. Ma, Y. Wang, H. Wang, Y. Zhao, Q. Wei, W. Yang, and C. Yang, "Fall preventive gait trajectory planning of a lower limb rehabilitation exoskeleton based on capture point theory," *Front. Inf. Technol. Electron. Eng.*, vol. 20, pp. 1322–1330, 2019.
- [9] C. Zhu and J. Yi, "Knee exoskeleton-enabled balance control of human walking gait with unexpected foot slip," *Robot. Autom. Lett.*, vol. 8, no. 11, pp. 7751–7758, 2023.
- [10] A. Vallinas, A. Keemink, C. Bayón, E. van Asseldonk, and H. van der Kooij, "Momentum-based balance control of a lower-limb exoskeleton during stance," in *Int. Conf. Rehabil. Robot*. IEEE, 2023, pp. 1–6.
- [11] T. Zhang, M. Tran, and H. H. Huang, "Nrel-exo: A 4-dofs wearable hip exoskeleton for walking and balance assistance in locomotion," in *Int. Conf. Intell. Robots Syst*. IEEE, 2017, pp. 508–513.
- [12] Z. Li, "Comparison between safety methods control barrier function vs. reachability analysis," *arXiv preprint arXiv:2106.13176*, 2021.
- [13] T. Gurriet, A. Singletary, J. Reher, L. Ciarletta, E. Feron, and A. Ames, "Towards a framework for realizable safety critical control through active set invariance," in *IEEE Int. Conf. Cyber-Phys. Syst.*, 2018, pp. 98–106.
- [14] A. Agrawal and K. Sreenath, "Discrete control barrier functions for safety-critical control of discrete systems with application to bipedal robot navigation," in *Robot. Sci. Syst.*, vol. 13. Cambridge, MA, USA, 2017, pp. 1–10.
- [15] Y. Zhou, J. Cheng, B. Chen, J. Zhou, K. Yue, and Z. Wang, "Cbf-based constrained optimization for safe and adaptive cpg gait planning in rehabilitation robots," in *Chin. Control Conf.* IEEE, 2025, pp. 5095–5100.
- [16] O. N. Beck, M. K. Shepherd, R. Rastogi, G. Martino, L. H. Ting, and G. S. Sawicki, "Exoskeletons need to react faster than physiological responses to improve standing balance," *Sci. Robot.*, vol. 8, no. 75, p. eadf1080, 2023.
- [17] R. M. Murray, Z. Li, and S. S. Sastry, *A Mathematical Introduction to Robotic Manipulation*. NW Boca Raton, FL: CRC press, 2017.
- [18] D. A. Winter, *Biomechanics and Motor Control of Human Movement*. John Wiley & Sons, 2009.
- [19] A. D. Ames, S. Coogan, M. Egerstedt, G. Notomista, K. Sreenath, and P. Tabuada, "Control barrier functions: Theory and Applications," in *Eur. Control Conf.* IEEE, 2019, pp. 3420–3431.
- [20] C. Curtze, T. J. Buurke, and C. McCrum, "Notes on the margin of stability," *J. Biomech.*, vol. 166, p. 112045, 2024.
- [21] M. Jacquelin Perry, "Gait analysis: normal and pathological function," *New Jersey: SLACK*, 2010.
- [22] Q. Nguyen and K. Sreenath, "Safety-critical control for dynamical bipedal walking with precise footstep placement," *IFAC-PapersOnLine*, vol. 48, no. 27, pp. 147–154, 2015.
- [23] W.-H. Chen, D. J. Ballance, P. J. Gawthrop, and J. O'Reilly, "A nonlinear disturbance observer for robotic manipulators," *IEEE Trans. Ind. Electron.*, vol. 47, no. 4, pp. 932–938, 2000.
- [24] M. Yu and G. Lv, "Task-invariant centroidal momentum shaping for lower-limb exoskeletons," in *Conf. Decis. Control*. IEEE, 2022, pp. 2054–2060.
- [25] R. Cham and M. S. Redfern, "Lower extremity corrective reactions to slip events," *J. Biomech.*, vol. 34, no. 11, pp. 1439–1445, 2001.
- [26] S. Madgwick *et al.*, "An efficient orientation filter for inertial and inertial/magnetic sensor arrays," *Report x-io and University of Bristol (UK)*, vol. 25, pp. 113–118, 2010.
- [27] H. M. Cho, I. Kang, D. Park, D. D. Molinaro, and A. J. Young, "Real-time walk detection for robotic hip exoskeleton applications," in *Proc. Int. Symp. Med. Robot*. IEEE, 2022, pp. 1–5.
- [28] B. Stellato, G. Banjac, P. Goulart, A. Bemporad, and S. Boyd, "OSQP: an operator splitting solver for quadratic programs," *Math. Program. Comput.*, vol. 12, no. 4, pp. 637–672, 2020.
- [29] H. Debelle, C. N. Maganaris, and T. D. O'Brien, "Biomechanical mechanisms of improved balance recovery to repeated backward slips simulated by treadmill belt accelerations in young and older adults," *Front. Sports Act. Living*, vol. 3, p. 708929, 2021.
- [30] R. Janna, K. Tarapongnivat, N. Sricom, C. Akkawutvanich, X. Xiong, and P. Manoonpong, "Online adaptive impedance control with gravity compensation for an interactive lower-limb exoskeleton," in *Int. Conf. Intell. Robots Syst*. IEEE, 2024, pp. 12793–12800.
- [31] P. R. Golyski, N. K. Swaich, F. A. Panizzolo, and G. S. Sawicki, "Effects of an elastic hip exoskeleton on stability quantified by mechanical energetics and whole-body angular momentum during walking with treadmill belt speed perturbations," *J. Biomech.*, p. 112784, 2025.
- [32] C. O'Connell, A. Chambers, A. Mahboobin, and R. Cham, "Effects of slip severity on muscle activation of the trailing leg during an unexpected slip," *J. Electromyogr. Kinesiol.*, vol. 28, pp. 61–66, 2016.
- [33] M. Afschrift, L. Pitto, W. Aerts, R. van Deursen, I. Jonkers, and F. De Groote, "Modulation of gluteus medius activity reflects the potential of the muscle to meet the mechanical demands during perturbed walking," *Sci. Rep.*, vol. 8, no. 1, p. 11675, 2018.
- [34] Vicon, *Plug-in-Gait Modelling Instructions*, Vicon Motion Systems, Oxford, UK, 2002, vicon Manual. Oxford Metrics Ltd.
- [35] A. Rajagopal, C. L. Dembia, M. S. DeMers, D. D. Delp, J. L. Hicks, and S. L. Delp, "Full-body musculoskeletal model for muscle-driven simulation of human gait," *IEEE Trans. Biomed. Eng.*, vol. 63, no. 10, pp. 2068–2079, 2016.
- [36] T. D. O'Brien, N. D. P. Reeves, V. Baltzopoulos, D. A. Jones, and C. N. Maganaris, "In vivo measurements of muscle specific tension in adults and children," *Exp. Physiol.*, vol. 95, no. 1, pp. 202–210, 2010.
- [37] T. Negishi and N. Ogihara, "Regulation of whole-body angular momentum during human walking," *Sci. Rep.*, vol. 13, no. 1, p. 8000, 2023.
- [38] M. Van Mierlo, J. Ambrosius, M. Vlutters, E. Van Asseldonk, and H. Van Der Kooij, "Recovery from sagittal-plane whole body angular momentum perturbations during walking," *J. Biomech.*, vol. 141, p. 111169, 2022.
- [39] H. Debelle, C. Harkness-Armstrong, K. Hadwin, C. N. Maganaris, and T. D. O'Brien, "Recovery from a forward falling slip: measurement of dynamic stability and strength requirements using a split-belt instrumented treadmill," *Front. Sports Act. Living*, vol. 2, p. 82, 2020.